The administration of exogenous HSP47 as a collagen specific therapeutic approach

Roberta Besio[1], Nadia Garibaldi[1]*, Alessandra Sala[1]*, Francesca Tonelli[1], Carla Aresi[1], Elisa Maffioli[2,3], Claudio Casali[4], Camilla Torriani[5], Marco Biggiogera[4], Simona Villani[5], Antonio Rossi[1], Gabriella Tedeschi[2,3], Antonella Forlino[1]

[1]Department of Molecular Medicine, Biochemistry Unit, University of Pavia, Pavia, Italy; [2]Department of Veterinary Medicine and Animal Sciences (DIVAS), University of Milan, Lodi, Italy; [3]CIMAINA, University of Milan, Milano, Italy; [4]Department of Biology and Biotechnology, University of Pavia, Pavia, Italy; [5]Department of Public Health, Experimental and Forensic Medicine, University of Pavia, Italy

*These authors contributed equally to the work

Corresponding Author:
Antonella Forlino, PhD
Department of Molecular Medicine, Biochemistry Unit
University of Pavia
Via Taramelli 3B
27100 Pavia, Italy
Phone: +39-0382-987235
e-mail: aforlino@unipv.it

Conflict-of-interest statement

The authors have declared that no conflict of interest exists.

Abstract

The proof-of-principle of the therapeutic potential of heat shock protein 47 (HSP47) for diseases characterized by defects in the collagen I synthesis is here proved in osteogenesis imperfecta (OI), a prototype of collagen disorders. Most of the OI mutations delay collagen I chains folding, increasing their exposure to post translational modifications that affect collagen secretion and impact extracellular matrix fibrils assembly. As model, we used primary fibroblasts from OI individuals with defect in the collagen prolyl-3-hydroxylation complex, since are characterized by the synthesis of homogeneously overmodified collagen molecules. We demonstrated that the exogenous recombinant HSP47 (rHSP47) is uptaken by the cells and localizes at the ER exit sites and ER Golgi intermediate compartment. rHSP47 treatment increased collagen secretion, reduced collagen post translational modifications and intracellular collagen retention and ameliorated the general ER proteostasis, leading to improved cellular homeostasis and vitality. These positive changes were also mirrored by an increased collagen content in the OI matrix. A mutation dependent effect was found in fibroblasts from three probands with collagen I mutations, for which rHSP47 was effective only in cells with the most N-term defect. A beneficial effect on bone mineralization was proved in vivo in the zebrafish *p3h1*$^{-/-}$ OI model.

Keywords: bone/collagen/HSP47/osteogenesis imperfecta

Introduction

Collagen type I, the most abundant protein in human body, provides tissues with the necessary structural and/or functional support. Collagen is synthetized as procollagen molecule in the ER where two proα1 and one proα2 chains assemble from the C-terminal end, to form a trimer with a central clockwise triple helix domain flanked by two globular N- and C- terminal propeptides (1). In the ER, procollagen I chains undergo post-translational modifications, including hydroxylation of triple helical and telopeptide lysine residues, performed by lysyl hydroxylase -1 and -2, respectively (2). Proline residues are also hydroxylated in C-4 and C-3 by prolyl-4-hydroxylase B and prolyl-3-hydroxylase complexes, respectively, the latter composed of prolyl-3-hydroxylase 1 (P3H1) associated in a 1:1:1 ratio with cartilage-associated protein (CRTAP) and cyclophilin B (CyPB) (2). Some hydroxylysines are then glycosylated by hydroxylysyl-galactosyltransferase and galactosyl-hydroxylysyl-glucosyltransferase that transfer a galactose unit to hydroxylysine residues and a glucose unit to galactosyl-hydroxylysine residues, respectively (3, 4). Then procollagen leaves the ER and moves to the Golgi intermediate compartment (ERGIC) in COP2 vesicles (5). Large cargo molecules as collagen require specialized factors to promote their packaging and exit from the ER. Kelch-like protein 12 (KLHL12) facilitates the collagen transport by binding to a COP2-component, SEC31, and triggering its monoubiquitinylation (6). Once in the Golgi, procollagen is transported in post-Golgi tubular saccular carriers by the detachment of large regions of the trans Golgi (7-9) and bundles of procollagen are then released to form secretory vacuoles (10). Following procollagen secretion, the pericellular removal of N- and C-propeptides allows the self-assembling of mature collagen molecules in extracellular matrix (ECM) fibrils (2, 10). Chaperones and several multiprotein complexes are involved in collagen biosynthesis (11), and among them heat shock protein 47 (HSP47) has multiple roles during the process. In the ER HSP47 interacts with the Gly-X-Arg and weakly with the Gly-Pro-Hyp

motifs at the N-terminal region of nascent procollagen polypeptide chains to help their folding and recognizes the folded triple-helical conformation, preventing local triple helical unfolding and intracellular aggregation (12). HSP47 also has a relevant role in secretion since it bridges procollagen to the ER transmembrane protein TANGO1, a key player in the formation of the COP2 vesicles used by procollagen to leave the ER (11).

Altered collagen I intracellular synthesis, secretion and extracellular processing and assembly characterize both physiological conditions such as aging, and pathological conditions like vitamin C deficiency, homocystinuria, osteoporosis and genetic diseases like Ehlers–Danlos syndrome and osteogenesis imperfecta (OI) (13-16). OI is usually referred to as brittle bone disease, since the primary clinical manifestations are skeletal deformity and fragility associated to reduced bone mass. Nevertheless, extra skeletal manifestations have been reported that include pulmonary function impairment, cardiac valve abnormalities, muscle weakness, blue sclerae, hearing loss, dentinogenesis imperfecta, and ligamentous laxity (14, 17). OI is a family of heritable collagen type I-related disorders, caused by defects in different genes, and it is often associated to matrix collagen insufficiency caused either by quantitative defect, due to reduced normal collagen I synthesis, or by intracellular retention of collagen molecules with an altered structure.

Currently, there is no effective therapy available for OI. Most of the treatments focus primarily on conservative and surgical intervention to improve the patients' quality of life and pharmacological therapy is still for the most based on bisphosphonates administration (18, 19). Despite their positive effects on bone mass, bisphosphonates decrease bone turnover and studies on humans and mice have raised concerns about the effect of high cumulative doses of the drug on bone remodelling and healing, especially in paediatric age (20-22). The development of anabolic approaches has been more recently proposed based on the possibility to increase collagen synthesis and thus bone mass. To this aim the anti-sclerostin antibody,

inhibiting the negative regulator of the WNT pathway in osteoblasts and recently approved for osteoporosis treatment by EMA and FDA, was used in OI animal models where it improved bone strength and microarchitecture, and reduced axial and long bone fractures (23-25). The same drug in phase 2a and 2b clinical trials has shown an increase in markers of bone formation, along with a decrease in bone resorption markers and a BMD gain at the lumbar spine. Unfortunately, cardiovascular safety concerns for major cardiovascular events were raised during the clinical trials (26), underling the need for new and safer therapeutic molecules.

Collagen biosynthesis and secretion strongly depend on the proper expression and function of the collagen-specific molecular chaperone HSP47 and hence it is tempting to hypothesize its possible use as OI drug. Unlike other heat shock proteins and other ER-resident proteins involved in collagen folding and maturation, HSP47 does not possess other known client proteins (27-29). The chaperone is expressed in all collagen-synthesizing cells, and constitutive expression levels correlate strictly with the amounts of collagen being synthesized. Administration of exogenous HSP47 could potentially exert a specific effect on collagen secretion in all collagen producing cells, thus this effect will address for the first time, and unlike other proposed treatments, all OI affected tissues.

Here we evaluated the therapeutic potential of a recombinant form of HSP47 (rHSP47) on OI patients' fibroblasts. As prototype defects for a first proof-of-concept of the efficacy of the HSP47 treatment in presence of collagen with abnormal structure we choose the recessive OI types VII (OMIM # 610682) and VIII (OMIM # 610915) caused by mutations in *CRTAP* and *P3H1*, respectively (30, 31), since, unlike the classical OI dominant cases associated to mutations in the collagen genes, cause the synthesis of collagen molecules with similar level of post translational modifications and thus constitute the ideal substrate for testing a drug acting on collagen folding and secretion.

The drug effect on collagen deposition was also evaluated in fibroblasts from patients with collagen I mutations in different positions along the chain. Lastly, bone mineralization was assessed upon rHSP47 treatment in vivo in a zebrafish OI model.

Results

rHSP47 reduces intracellular procollagen I retention

Exogenous rHSP47 cellular uptake was first proved in control human fibroblasts by confocal microscopy using its GFP covalently linked form (rHSP47-GFP+) (Figure 1A). Surprisingly, co-immunolabelling showed no localization of rHSP47-GFP+ either with the ER lumen marker protein disulfide isomerase (PDI) or the ER membrane marker calnexin (Figure 1, B and C). Co-localization of rHSP47-GFP+ with specific sites of the secretory pathway, namely *cis*-Golgi (GM130) and secretory vesicles (COP2 and KLHL12), was instead found (Figure 1, D-F).

The therapeutic potential of rHSP47 was then evaluated on OI patients' fibroblasts. Primary fibroblasts from three previously described recessive OI patients with mutations in the components of the collagen 3-prolyl hydroxylation complex (32, 33) were selected for the study (Table 1). As expected based on previous data (31), a strong intracellular procollagen accumulation together with higher level of the ER marker PDI were observed in type VII and VIII OI proband primary fibroblasts compared to controls (Figure 2, A-C). The abnormal collagen strongly co-localized with PDI (Figure 2, D and E). rHSP47 incubation significantly decreased the amount of intracellular collagen, to the level of control fibroblasts, in all mutant fibroblasts.

rHSP47 ameliorates cell homeostasis in OI probands' fibroblasts by increasing collagen I secretion

The effect of rHSP47 was evaluated also on general ER proteostasis by treating cells with the protein aggregate-binding fluorescent molecule thioflavin T (ThT) (34, 35). Enhanced ThT fluorescence was found in all proband cells compared to controls, demonstrating the intracellular accumulation of misfolded material that was significantly reduced following

rHSP47 treatment (Figure 3, A and B). The impact of rHSP47 on intracellular protein aggregates was also mirrored by impressive improvement in cellular morphology: the ER cisternae, enlarged in mutant cells, normalized after treatment (Figure 3, C and D). The impaired proteostasis severely affects vitality in OI cells, often inducing apoptosis activation (30, 31, 36-39). rHSP47 treatment decreased the number of apoptotic cells, when an increased amount was present, as in proband 1, while did not affect vitality in the other cases (Figure 4, A and B). Of relevance, upon the induction of a high stress condition by culturing the cells for 7 days without media change, the positive effect of the treatment was even more pronounced on cell viability. Indeed, a strong decrease of the population of late apoptotic cells, and an increase of the percentage of early apoptotic and live cells was evident in mutant cells treated with rHSP47 (Figure 4, C and D).

The impairment of the collagen prolyl 3-hydroxylation complex in primary human fibroblasts decreases collagen I secretion leading to a matrix insufficiency (31). Thus, secreted collagen I was quantified in culture media in absence or presence of rHSP47 (Figure 5A). A significant increased amount of collagen content following rHSP47 incubation was evident in all the samples. ^{3}H-labeled collagen I pulse-chase experiment performed in fibroblasts form proband 1 further confirmed the chaperone stimulatory effect on collagen I secretion (Figure 5B).

rHSP47 improves the quality of the secreted collagen molecules and their presence in the matrix

The impairment of the collagen prolyl 3-hydroxylation complex affects collagen I folding, causing increased collagen hydroxylation and glycosylation (14). In all analyzed OI probands cells, the presence of collagen overmodifications was confirmed by electrophoretic analysis of ^{3}H-labeled collagen I. Steady-state collagen gels revealed the broadening and delay of the α bands typical of excessive glycosylated collagen I. rHSP47 incubation slightly reduced the α(I)

bands broadening, suggesting a reduced collagen post translational modification level (Figure 5C). To evaluate lysyl hydroxylation and lysine O-glycosylation along the collagen helix, collagen extracted from control, OI proband 3 and rHSP47-incubated OI proband 3 cells was subjected to trypsin digestion and tandem mass spectrometry analysis was performed. Several hydroxylysine (Hyl) and galactosyl-hydroxylysine (GHL) and glucosylgalactosyl-hydroxylysine (GGHL) sites were identified by LC-MS/MS analysis: 4 Hyl (K^{252}, K^{270}, K^{327}, K^{603}), 1 GHL (K^{99}) and 4 GGHL sites (K^{87}, K^{99}, K^{408}, K^{855}) were detected in the α1 chain; and 4 Hyl (K^{264}, K^{270}, K^{408}, K^{567}) and 4 GGHL sites (K^{87}, K^{264}, K^{564}, K^{648}) were detected in the α2 chain (Figure 5D, Table 2 and Supplementary Table S1). The abundance of peptides containing Hyl and the abundance of GHL/GGHL peptides, as well as of the corresponding unmodified peptides, were calculated using Skyline software to compare the peaks intensity across the specimen. The ratio between the peak intensity of modified peptides and the total intensity of all corresponding peptide's forms (unmodified + hydroxylated + mono-O-glycosylated + di-O-glycosylated) indicated an increased O-glycosylation of both collagen α1(I) and α2(I) chains in OI proband cells. The incubation with rHSP47 significantly reduced collagen lysine hydroxylation and O-glycosylation at several residues. The lysine hydroxylation/ratio was reduced at α1-K603 and at α2-K264 and -K270, the galactosylated ratio and galactosyl-glucosylated ratio were reduced at α1-K99 and at α1-K408, respectively, while α2-K264, -K564 and –K648, values were closed to control (Table 2). No changes were detected at α1-K87 and α2-K87, relevant sites for collagen cross links.

Collagen triple helix structure before and after treatment was assessed by circular dichroism monitoring collagen ellipticity at different wavelengths. An ellipticity change in the negative band at 200 nm, sensitive to triple helix structure (40), was evident in the CD spectra of collagen from proband 3 compared to control, supporting the abnormal structure of mutant

collagen. Confirming a positive effect of HSP47 on collagen I structure, the mutant collagen ellipticity at 200 nm return to control values upon rHSP47 treatment (Figure 5E).

To quantify the amount of collagen I incorporated into the ECM, upon decellularization, collagen staining was performed with picro sirius red, a strong anionic dye that binds preferentially to the cationic groups of collagen. The spectroscopic quantification of the dye clearly revealed a significant increase of collagen in all probands' ECM (Figure 5F). The collagen content in the ECM of proband 1 treated with rHSP47 was even greater than the collagen of controls, underling the relevance of choosing a proper dose to avoid in vivo an excessive collagen production and thus fibrosis.

The drug effect on collagen deposition was then evaluated, upon cell decellularization, also in fibroblasts from patients with the following collagen I mutations: α(I)G478S, α(I)G667R and α(I)G994D. While in α(I)G478S fibroblasts with the most N-term mutation we found a positive effect of rHSP47, no effect was found in α(I)G667R and α(I)G994D, cells with more C-term mutations (Figure 5G), suggesting that the effect of the treatment is likely mutation dependent.

rHSP47 improves mineralization in zebrafish larvae

To investigate in vivo the effect of exogenous rHSP47 on the skeleton, we took advantage of the zebrafish *p3h1*$^{-/-}$, recently generated and characterized in our laboratory as valid model for recessive OI type VIII. Indeed, *p3h1*$^{-/-}$ larvae are characterized by head disproportion and by an impaired cranial bones mineralization starting from the first weeks post fertilization (wpf) (41). From 1 to 11 days post fertilization (dpf) *p3h1*$^{-/-}$ embryos were treated every other day with a 4 hour pulse of 0.5 μM rHSP47 (Figure 6A). Analyses of the fish morphology at 11 dpf revealed no effect on the head disproportion since the ratio snout-operculum length/ height at eye was unaffected by the treatment (Figure 6B). At 11 dpf bone mineralization was also evaluated by alizarin red S staining. Three classes of mineralization were defined, namely

beginning/no mineralization, incomplete and complete, based on the level of alizarin red staining. The staining revealed a significant increased mineralization of notochord (NC), ceratohyal (CH) and 5th ceratobranchial (Figure 6, C-F), cranial bone characterized by perichondral, and endochondral ossification, respectively. Furthermore, the spectrophotometric quantitation of the total larvae mineral content confirmed the significantly increased mineralization upon rHSP47 incubation (Figure 6G).

Discussion

The reported data provides the proof-of-principle for exogenous recombinant heat shock protein 47 (rHSP47) administration as promising treatment for diseases characterized by poor collagen I secretion and matrix incorporation. Both in vitro and in vivo approaches using osteogenesis imperfecta (OI) type VII (33, 42) and VIII (43) human fibroblasts and a zebrafish OI type VIII model (*p3h1*$^{-/-}$) (41), respectively, support our conclusions. Mutant fibroblasts incubation with rHSP47 reduced collagen post translational modifications (PTMs), increased collagen secretion and matrix incorporation, and ameliorated the general ER proteostasis, leading to an improved cellular homeostasis and vitality. These positive cellular effects translated in vivo in a significant improved bone mineralization. Of note, a mutation dependent effect was found in fibroblasts from probands with collagen I mutations where the treatment was effective only in cells with the most N-term mutation.

Collagen I retention and its only partial secretion from the ER causing a defective extracellular matrix deposition are common features in dominant OI types carrying mutations in collagen I genes and in several recessive OI forms characterized by collagen structural defects (31, 36-38, 44-46). Furthermore, reduced collagen synthesis and matrix insufficiency are hallmarks of aging related skeletal diseases such as osteoporosis, thus representing appealing pharmacological targets to ameliorate human health and reduce health care national system expenses in an aged society. Despite that, the search for therapies addressing these targets is still exiguous. The anti-sclerostin antibody, the only currently available drug approved for osteoporosis and in clinical trials for OI that enhances collagen deposition does not specifically target collagen but, being an inhibitor of the WNT pathway, exerts an effect on other essential cellular functions, with potential serious side effects (47, 48). Similarly, lack of collagen specificity characterizes the most recent anti-TGFβ antibody treatment that is in clinical trials as inhibitor of tumor microenviroment and metastasis and as bone mineral density inducer for

OI (49). In the last decade, in vitro and in vivo preclinical studies by us and others, identified in the chemical chaperone 4-phenylbutyrate (4-PBA) a new anabolic drug able to ameliorate OI osteoblast homeostasis and skeletal properties both in a zebrafish and in two murine models of dominant OI (50-52). In vitro study using Chinese hamster ovary cells revealed that 4-PBA promotes proper COP2 coat assembly, known to be necessary for ER large proteins, including collagen I molecules, transit from ER to the Golgi (53). Nevertheless, 4-PBA, similarly to the above-mentioned anabolic drugs in clinics or clinical trials, is not specific for collagen and does not affect the OI altered collagen structure.

The chemical chaperone HSP47 specifically interacts with collagen I, facilitating its folding, limiting its intracellular aggregation and allowing its secretion. Thus, taken this information into account, we reasoned that HSP47 administration could fill the lack of drugs specifically targeting collagen I synthesis, modulating its PTMs levels and favoring its secretion (28, 54). The expression of HSP47 correlates with collagen deposition (28). On the other hand, knocking out HSP47 expression in mouse embryos results in abnormally oriented epithelial tissues and in ruptured blood vessels due to severe deficiency in mature forms of type I and type IV collagen leading to a lethal phenotype (55), while in humans homozygosity for a missense mutation causes a recessive moderate to severe form of OI with distinct effect on collagen I secretion and structure depending on the type of defect (56).

While rHSP47 administration to healthy individuals may be detrimental because elevated expression of HSP47 is observed in a variety of fibrosis models (57) and has been associated to the promotion of cancer (58), administration to individuals with impaired collagen secretion would potentially help to overcome matrix insufficiency.

Our data demonstrated the cellular uptake of an exogenously provided recombinant form of HSP47 in human fibroblasts, providing new information regarding its localization. The HSP47 RDEL C-terminal motif is known to bind to the KDEL receptor (KDELR) in the ER-Golgi

intermediate compartment, but KDELRs are also present in the plasma membrane (PM) (59). Following ligand interaction, the PM located KDELR1 was proved to be endocytosed to early endosomes via clathrin mediated endocytosis before entering the Golgi and then be recycled back to the endosomal compartment or to the PM (59). The rHSP47-GFP^{+} co-localization with COP2, KLHL12 and GM130 by immunofluorescence proved its presence at the ER exit site (ERES). ERES, specific exit points for ER synthesized proteins, are specialized membrane domains on the surface of the ER that are identified by the COP2 heterocomplex and ER-Golgi recycling proteins such as ERGIC53 (60). The procollagen molecules are recruited to the ERES by the ERES resident protein TANGO1, whose SH3 domain is bound by HSP47 interacting with procollagen triple helix (28, 61). A recent model for procollagen secretion proposed an active role of proton and HSP47 concentration gradient existing between ERES and *cis*-Golgi in generating the necessary biomechanical driving force to allow procollagen through tunnels present between ER and Golgi (5). The localization of rHSP47 at the ERES site could indeed explain a higher concentration gradient possibly responsible for the increased rate of collagen secretion detected in treated mutant fibroblasts. HSP47 is known to preferentially bind to folded triple helix procollagen stabilizing an otherwise thermally unstable molecule, whereas PTMs are reported to occur on the unfolded collagen chains and to be blocked from their winding (62). Thus, quite unexpectedly, the exogenous rHSP47 decreased collagen hydroxylation and glycosylation, as demonstrated by MS data. An intriguing explanation could be a feedback effect of the increased presence of exogenous rHSP47 on the transcription/translation of other PTMs enzymes and chaperones. It has been recently reported that, in a recessive OI patient carrying a mutant HSP47-R222S, collagen I was over glycosylated likely due to an increased expression of chaperones and modifiers compensating for the abnormal HSP47 collagen I binding (63). The authors hypothesized that presumably those proteins were occupying the vacant HSP47 binding sites causing collagen over

modification. Another possible explanation could be the existence of relevant collagen PTMs in the ER-to-Golgi transition tunnel where the triple helices are already assembled, but where HSP47 is starting to be released due to lowering of the pH. Indeed, it has been discovered a post-Golgi trafficking mediated by VIPAR that is essential for modification of lysine residues by lysyl hydroxylase 3 (LH3) in multiple collagen types, including type I (64). Thus, it is possible that the faster collagen secretion upon HSP47 treatment reduces also the time for LH3 collagen modifications.

The rHSP47 incubation is particularly promising for OI treatment since it proved to specifically target at least three hallmarks of OI, namely it reduces PTMs, it increases collagen synthesis limiting intracellular retention and it increases the collagen amount in ECM. Nevertheless, our findings also reveal the need for optimizing dose and time of treatment. For instance, the collagen I content in the ECM of proband 1 treated with rHSP47 is even greater than the collagen amount of controls, as well as the levels of GHL and GGHL in α1(I) upon treatment are reduced to levels even lower than control, underling the relevance of the choice of a proper dose to avoid in vivo an excessive collagen production and thus fibrosis or the synthesis of an undermodified collagen molecules. Of relevance, collagen undermodification, a peculiar feature found in OI type XIV patients, is detrimental for bone properties as well as its overmodification.

The efficacy of the treatment was here first tested in probands with mutations impairing the collagen prolyl 3-hydroxylation complex and causing the synthesis of collagen molecules with similar level of PTMs. OI types caused by mutations in the collagen prolyl 3-hydroxylation complex, and in few other genes encoding for proteins involved in collagen folding and post translational modifications (i.e. *FKBP10*, *MESD*, *PLOD*), are the more common among the recessive OI forms, representing more than 880 individuals (65). Nevertheless, the findings that the effect of the treatment is likely mutation dependent in case of collagen I mutations, and

370 that, perhaps for patients with more C-term mutation, and higher PTMs level, the effective
371 HSP47 dose could be different, or the treatment could be less effective, represent a potential
372 limit of the proposed treatment. Indeed, the position of the mutation, the type of substituting
373 amino acid and the affected chain result in collagen with heterogeneous modifications, and this
374 can be responsible for the different response. Furthermore, the translatability of these
375 promising positive effects from fibroblasts to osteoblasts, that are known to synthesize higher
376 collagen amounts, is still pending. For instance, working with iPS cells isolated from OI
377 patients and differentiated toward osteoblasts could provide additional useful insights.
378 Besides bone and skin, collagen I is present in the connective tissues of many other organs
379 providing the tissue with tensile strength. In particular, it is present in all major structures of
380 lung, in the skeletal muscle where it accounts for 1–10% of its mass dry weight and it plays an
381 important role in muscle fiber force transmission, and it is a major component of cardiac valves
382 and aortic wall and its altered synthesis can affect their biomechanical properties (66), leading,
383 in rare cases, to aortic dissection (67). The use of exogenous rHSP47 as OI treatment, unlike
384 other proposed drugs, could target all OI affected tissues likely improving also the extra skeletal
385 manifestations of the diseases, a major concern for adult patients (68). Of relevance, being
386 HSP47 a specific chaperone for fibrillar collagen, the same therapeutic approach could be
387 applied to several other conditions in which collagen synthesis is impaired, either genetically
388 or acquired due to environmental factors, such as epidermolysis bullosa (69), Ehlers-Danlos
389 syndrome (15), chondrodysplasia (70, 71) or UV exposure (72) and smoking (73-75).
390 Our study demonstrated the power of exogenous rHSP47 in ameliorating cellular homeostasis
391 and bone mineralization using in vitro and in vivo models of recessive OI forms characterized
392 by collagen post translational over modifications. The unchanged disproportion in *p3h1*$^{-/-}$
393 treated larvae underlines the need to evaluate the effect of a long-term treatment for which a
394 specific delivery system for the recombinant protein is necessary.

The identification of specific therapies for the different OI forms, or even for specific group of mutations in the same gene, is the seed for the development of a personalized medicine approach with the final aim to ameliorate OI individual quality of life.

Although the analyses of rHSP47 effect on bone fragility and of the possible side effects of a high HSP47 level demand a deep dose-effect *in vivo* investigation, our results pave the way for a new pharmacological approach for OI as well as for other rare and common disorders associated to collagen deficiency.

Materials and methods

Sex as a biological variable

Our study examined skin biopsies from male (n = 1) and female (n = 2) individuals with OI and individuals without disease acting as controls. Sex was not considered as a biological variable. For zebrafish embryonic/juvenile experiments, clutch-matched fish were randomly assigned to each treatment group and used without sex bias.

rHSP47 expression and purification

Recombinant HSP47 protein (rHSP47), non-conjugated and conjugated with EGFP was kindly provided by Dr Hambardzumyan and by Dr Khan (INM-Leibniz Institute for New Materials, INM, Campus D2 2, Saarbrück, Germany). A construct encoding amino acids 36–418 of the canine HSP47 (canine *SERPINH1* mRNA, NCBI accession NM_001165888), was cloned into the pET22-(b) vector (Novagen) with a C-terminal hexahistidine tag. Proteins was expression in BL21(DE3) cells and purified by Ni-NTA affinity chromatography (Ni-NTA superflow; Qiagen). The eluate was reduced with 4 mM DTT, and 1.5 M ammonium sulphate was added to precipitate contaminants. The soluble fraction was concentrated and purified further by gel filtration (Superdex S75; GE Healthcare) in 20 mM Hepes pH 7.5, 300 mM NaCl, 4 mM DTT.

Human fibroblasts culture and rHSP47 treatment

Human primary dermal fibroblasts from skin biopsies of pediatric OI probands carrying mutations in one of the genes coding for the members of the collagen prolyl 3-hydroxylation complex, CRTAP (OI type VII (33, 42)) or P3H1 (OI type VIII (43)) (Table 1), and in collagen I α1 chain (α1(I)G478S, α1(I)G667R, α1(I)G994D) (76), were obtained after informed consent. All the primary cells were isolated and grown at the department of Molecular Medicine of the University of Pavia, Italy, with the exception of CRTAP mutant cells that were isolated at the

Department of Physiology and Cell Biology of the University of Arkansas for Medical Sciences, Little Rock, USA. Three aged, matched controls (Promo Cell) were selected. All cells were used at passages 7-12 (P7-12). Cells were grown at 37°C in humidified atmosphere containing 5% CO_2 and cultured in Dulbecco's modified Eagle's medium (DMEM, Lonza) supplemented with 10% foetal bovine serum (FBS, Euroclone), 4 mM glutamine (Euroclone). For each experiment 2.5×10^4 cells/cm² were plated and cultured in DMEM 10% FBS, 50 µg/ml ascorbic acid. Cells were harvested after 5 days. For treatment, cells were incubated with 0.5 µM rHSP47 (dissolved in phosphate buffer saline, PBS) or with placebo (same volume of PBS) for 16 h with the exception of collagen secretion and matrix incorporation experiments, for which cells were subjected to a 4 hour (h) pulse incubation with rHSP47/placebo every other day. After each treatment, cells were washed three times with PBS and fresh medium was added. For HSP47 localization, cells were incubated with 0.5 µM EGFP-rHSP47 (dissolved in PBS) for 4 h.

Immunofluorescence for intracellular localization

Collagen localization

Human primary fibroblasts were plated on glass coverslips (Marienfeld) and after 24 h treated with 0.5 µM rHSP47 for 16 h. For collagen localization studies, cells were fixed in 10% neutral buffered formalin. For collagen colocalization with the ER marker protein disulfide isomerase (PDI) and with the Golgi marker *cis*-Golgi matrix protein 130 (GM130), cells were sequentially incubated o/n with 1:100 collagen I α1 chain (Developmental Studies Hybridoma Bank, SP1.D8), 1:200 PDI (Cell Signaling, 3501S) and 1:100 AlexaFluor 647 conjugated anti-GM130 (BD Pharmingen, 558712) antibodies. The secondary antibodies AlexaFluor 546 goat anti-mouse IgG (Invitrogen, A-11030) and AlexaFluor 488 conjugated F(ab') fragment anti-rabbit IgG (Immunological Sciences, IS20013) were used at 1:400 dilution. Nuclei were

stained with 4',6-diamidino-2-phenylindole (DAPI, Sigma-Aldrich) and images were acquired by confocal microscope TCS SP8 (Leica). The total area of punctate signal per cell and signals colocalization were measured by the Leica software LAS 4.5.

rHSP47 localization

Human primary fibroblasts were plated on glass coverslips and after 24 h treated with 0.5 μM rHSP47-GFP$^+$ for 16 h. In order to evaluate rHSP47-GFP$^+$ colocalization with the endoplasmatic reticulum (ER), immunofluorescence experiments for the ER matrix marker PDI and ER membrane marker calnexin were performed. After cell fixation with formalin, cells were blocked with 1.5% bovine serum albumin (BSA), 0.3% Triton X-100 in PBS for 1 h at room temperature (RT). Antibody against PDI (Cell Signaling, 3501S) or against calnexin (Cell Signaling, 2679) was incubated overnight at 4°C using 1:200 dilution in blocking solution. Cells were sequentially incubated with goat anti-rabbit IgG DyLight 633 secondary antibody (Thermofisher, 35562), 1:400 dilution in blocking solution, for 2 h at RT.

To evaluate rHSP47-GFP$^+$ colocalization with Golgi apparatus, immunofluorescence for GM130 was performed. Cells were blocked with 0.5% BSA, 0.05% saponin, 50 mM NaCl and 15 mM glycine, pH 7.4, for 1 h at RT. Alexa Fluor 647 conjugated anti-GM130 (BD Pharmingen, 558712) was used at 1:100 dilution in blocking solution and incubated overnight at 4°C.

To evaluate rHSP47-GFP$^+$ colocalization with secretory vesicles, immunofluorescences for coat protein complex 2 (COP2), and kelch like family member 12 (KLHL12) were performed. For COP2 immunodetection, cells were permeabilized with 0.1% Triton X-100 dissolved in TBS and blocked with 3% BSA for 1 h at RT. Antibody against COP2 (Invitrogen, PA1-069) was used at 1:200 dilution in blocking solution and incubated overnight at 4°C. Cells were sequentially incubated with goat anti-rabbit IgG DyLight 633 secondary antibody (Thermofisher, 35562) at 1:400 dilution in blocking solution, for 2 h at RT.

For KLHL12 immunodetection, cells were blocked with 0.5% BSA, 0.05% saponin, 50 mM NaCl and 15 mM glycine, pH 7.4, for 1 h at RT. Antibody against KLHL12 (Sigma Atlas Antibodies, HPA07132) was used at 1:400 dilution in blocking solution and incubated overnight at 4°C. Cells were sequentially incubated with goat anti-rabbit IgG DyLight 633 antibody (Thermofisher, 35562) at 1:400 dilution in blocking solution, for 2 h at RT. Nuclei were counterstained with DAPI and images acquired by confocal microscope TCS SP8 (Leica) with 63x magnification. The co-localization analyses were performed with ImageJ software.

Thioflavin T labelling for protein aggregate analysis

Cells were plated on glass coverslips and cultured for 4 days before incubation with 5 mM Thioflavin (ThT, Sigma-Aldrich) for 16 h in presence or absence of rHSP47. Cells were then fixed with 4% paraformaldehyde (PFA) and nuclei were stained with DAPI. Images were acquired by confocal microscope TCS SP8 (Leica). The total area of punctate signal per cell was measured using the Leica software LAS4.5.

Transmission electron microscopy to evaluate ER morphology and cisternae size

For transmission electron microscopy analysis, fibroblasts were trypsinized, fixed in 2.5% glutaraldehyde for 2 h at RT, post-fixed in 2% (w/v) OsO_4 for 2 h at RT, and embedded in 2% agarose. The specimens were dehydrated in graded acetone, infiltrated with epoxy resin and finally polymerized in gelatin capsules. Ultrathin sections were cut on a Reichert OM-U3 ultramicrotome, collected on 300-mesh nickel grids, and stained with saturated aqueous uranyl acetate and lead citrate. JEM 1200 EX II electron microscope, operated at 100 kV and equipped with a MegaView G2 CCD camera was used for acquisition. ER cisternae thickness was measured with the built-in software on 30 cells per condition.

Fluorescence-activated cell sorting assay for cell viability and apoptosis evaluation

To determine rHSP47 effects on cell viability and apoptosis, cells were stained with annexin V – FITC conjugate and propidium iodide (PI) using FITC annexin V/dead cell apoptosis kit (Invitrogen, V13242). Samples were analyzed by fluorescence-activated cell sorting (BD FACS Lyric, Becton Dickinson). 1 x 10^4 events for each sample were considered measuring the fluorescence emission at 515-545 nm (FITC) and 675-715 nm (PI), to avoid fluorescence spillover. The BD FACS Suite (v1.3) software supplied by the manufacturer was used for the analysis.

Collagen quantification from cells media and extracellular matrix

Cells were cultured for 7 days and incubated with 0.5 µM rHSP47 pulse for 4 h every other day. On day 7, 24 h media was collected and, following PBS washing, the matrix was decellularized by incubation for 10 minutes in 50 mM Tris-HCl, pH 8.0 containing 2 M KCl and 0.2% TritonX-100. The decellularized matrix was extensively washed with 10 mM Tris-HCl, pH 8.0. DNA extraction was performed to confirm decellularization. Collagen extraction and quantification from medium and decellularized matrix was performed using SircolTM Soluble Collagen Assay (Biocolor).

Collagen steady state and chase analysis

Labelling of collagen with L-[2,3,4,5-^{3}H]-proline (PerkinElmer) was used to evaluate collagen overmodification and collagen secretion kinetic. 2.5×10^5 fibroblast cells were plated in 6 wells plate and grown for 24 h. Cells were then incubated for 2 hours with serum-free D-MEM containing 100 µg/ml ascorbic acid (Fluka) to stimulate collagen production (pre-labelling medium). For steady state experiments the labelling lasted for 18 h in the same media using 20 µCi of ^{3}H-Pro/well.

For chase experiments the labelling was performed for 4 h using 1.65 µCi of ^{3}H-Pro/ml, then the labelling media was replaced with serum-free D-MEM containing 2 mM proline (Sigma-Aldrich), 4 mM glutamine, 100 µg/ml penicillin and streptomycin and 100 µg/ml ascorbic acid (chase media). Collagen was collected at 0.5, 1, 2 and 3 h after the pulse. Collagen I from both medium and cell layer fractions was extracted as previously described (77). The radioactivity (counts for minute, CPM) was measured using a liquid scintillation counter (Tri-Carb 2300 TR). For steady state, the same amount (CPM) of ^{3}H-labeled collagen from each sample was denatured and run on 6% SDS-urea-PAGE. For chase analyses the same volume of ^{3}H-labeled collagens from each time point was electrophoresed. The gels were fixed in 45% methanol, 9% glacial acetic acid, incubated for one hour with enhancer (PerkinElmer), washed in deionized water. Gels were dried and placed in contact with a radiography film at -80°C. Films were developed, and the α(I) band intensity was evaluated using ImageQuant TL analysis software (GE). For chase analyses the ratio between the collagen in the media and the total collagen (medium plus cell layer) was evaluated.

Mass spectrometry analysis of collagen I post translational modifications

nLC-MS/MS analysis was used to assess hydroxylation and O-glycosylation of lysine sites of collagen I. Collagen I was extracted, as reported above, from culture media of control, OI proband 3 and rHSP47 treated OI proband 3 primary fibroblasts incubated o/n with 50 µg/ml ascorbic acid to stimulate collagen secretion. Media from 3 T25 confluent flask for each condition were collected every other day for three times and pulled. Collagen was quantified, separated by SDS-PAGE and stained with colloidal Coomassie; the α1(I) and α2(I) bands were excised and destained in 0.1% trifluoroacetic acid (TFA): acetonitrile (ACN) 1:1 (v/v) (78). Each band was reduced, alkylated, and digested o/n with trypsin sequence grade (Promega, T7575) at 37 °C using a protease:protein ratio (1:10) (79). Proteolytic digests were extracted

with 50% ACN in 0.1% TFA and desalted using µZip-Tip C18 (Pierce, 87784) before MS analysis (80). NanoHPLC coupled to MS/MS analysis was performed on Dionex Ultimate 3000 HPLC system with an EASY-SprayTM 2 µm 15 cm × 150 µm capillary column filled with 2 µm C18 100 Å particles, connected to a Q-Exactive Orbitrap (Thermo Fisher Scientific). MS spectra were collected over an m/z range of 350 – 2000 Da at resolution of 70,000, operating in the data dependent mode. HCD MS/MS spectra were collected at resolution of 17,500 for the 10 most abundant ions in each MS scan using a normalized collision energy of 35%, and an isolation window of 3 m/z. Rejection of +1 and unassigned charge states were enabled.

The acquired MS/MS spectra were searched against the UniProtKB/Swiss-Prot type I Collagen sequence database (release 2023_10) for Homo sapiens using Skyline software v23.1. Search parameters included: digestion by trypsin with a maximum of four missed cleavage sites, a minimum peptide length of 7, and a mass deviation of 10 ppm for monoisotopic precursor ions and 0.5 Da for MS/MS peaks. Carbamidomethylcysteine (+57.0236) was set as a fixed modification, while, Met oxidation (+15.994916), Lys hydroxylation (Hyl +15.994916), Lys galactosyl hydroxylation (GHL +178.047738) and glucosyl galactosyl hydroxylation (GGHL +340.100562) were set as variable modifications. The peak heights of the monoisotopic extracted ion chromatograms (XICs) of the Hyl and GHL/GGHL peptides of type I collagen (α1(I) and α2(I)) from control, OI and HS47 OI treated fibroblasts were compared, as well as the peak heights of the corresponding unmodified peptides. The ratio between the peak intensity of the modified peptides and the total intensity of all peptide's forms (unmodified + hydroxylated + mono-O-glycosylated + di-O-glycosylated) was calculated.

Collagen circular dichroism to analyse triple helix structure

Collagen was extracted from culture media of control, OI proband 3 and rHSP47 treated OI proband 3 primary fibroblasts incubated o/n with 50 µg/ml ascorbic acid to stimulate collagen

secretion. Collagen I was precipitated with half volume of 96% ethanol and digested overnight at 4°C with 100 µg/ml pepsin in 0.5 M acetic acid. The collagen was then precipitated with 2 M NaCl, in 0.5 M acetic acid and resuspended in 0.02 M acetic acid. All collagen I samples were prepared to a final concentration of 0.05 µg/µL. Circular dichroism (CD) spectra were acquired using a J-1500 spectrophotometer (Jasco). The measurements were performed at 4 °C, evaluating ellipticity as a function of wavelength in a range between 185 nm and 260 nm.

Alizarin red staining of zebrafish skeleton

WT AB zebrafish were obtained by European Zebrafish Research Center (Germany). *p3h1*$^{-/-}$ fish were generated in our laboratory (41) and bred in-house at the animal facility Centro di Servizio per la Gestione Unificata delle Attività di Stabulazione e di Radiobiologia of the University of Pavia, Pavia, Italy.

Adult zebrafish (AB) were kept into the ZebTec (Tecniplast) semi closed recirculation housing system at 28 °C, conductivity 500 µS, pH 7.5, and 14:10 hours light:dark cycle in the centralized animal facility of the University of Pavia. Zebrafish embryos were collected in 1.2 mM $NaHCO_3$, 0.1 g/L instant ocean, 1.4 mM $CaSO_4$, 0.00002% (w/v) methylene blue and kept at 28 °C into an incubator (Animal Protocol Approval No. 1191/2016). Zebrafish *p3h1*$^{-/-}$ embryos were obtained by mating *p3h1*$^{-/-}$ fish.

Upon mechanical chorion removal, embryos were treated every other day with 0.5 µM rHSP47 (dissolved in PBS) or placebo (same volume of PBS) for 4 h. Following the treatment, the fish water was changed with fresh water. The skeleton of 11 days post fertilization (dpf) larvae untreated (n=41) and treated (n=42) was stained as previously described with alizarin red S in order to assess the rHSP47 effect on mineralization (41). Images were acquired using a Leica M165 FC microscope connected to a Leica DFC425 C digital camera. Analyses of the fish morphology was carried out measuring the snout-operculum length, the height at eye and the

ratio snout-operculum length/ height at eye. The level of ossification of notochord (NC), ceratohyal bone (CH) and 5th ceratobranchial (5CB) was qualitatively described from beginning/incomplete to complete ossification based on the intensity of the staining from three independent operators blinded about the treatment groups. Total alizarin was also quantified by spectroscopic detection at 405 nm following the dissolution in 10% acetic acid at 85°C for 10 minutes. Alizarin red standards from 20 μM to 200 μM were used. Using lateral images snout operculum length, defined as the distance from snout to the most posterior point of operculum and height at eye, defined as the distance from ventral to dorsal, immediately posteriorly to the eye and perpendicularly to the body axis, were measured.

Study approval

Zebrafish studies were approved by the Italian Animal Research Council under the Protocol 260/2020-PR.

Statistical analysis

The aim of the present study was to describe the effect of genotype and rHSP47 treatment on several cellular and morphological parameters. An exploratory study design in vitro and in vivo using a zebrafish OI model was applied. The quantitative variables were expressed as mean and standard deviation (SD). Differences between rHSP47 treatment and placebo in cellular and morphological quantitative as well as pseudo-quantitative parameters were explored by Mann Whitney Wilcoxon test (MW test). Aligned rank ANOVA (ARA) equivalent to two-way ANOVA was applied to explore differences in collagen I, PDI, collagen I-PDI and thioflavin by treatment and genotype. Post-hoc analysis of the genotypes with respect to controls was conducted if nonparametric ARA was significant: Bonferroni's multiple comparisons correction was applied. To describe the effect of rHSP47 and genotype on secreted collagen,

matrix collagen and vital parameters, the analyses were conducted using MW test stratifying by genotype and comparing rHSP47 treatment and placebo due to the small number of experimental units. Kruskal-Wallis test was also applied to describe the secreted collagen by genotype. A p-value <0.05 was considered significant apart from the multiple comparisons test. All the analyses were conducted in STATA 17® and summarised in Supplementary Table S2.

Data Availability

Values for all data points in graphs are reported in the Supporting Data Values file.

The mass spectrometry proteomics data have been deposited to the ProteomeXchange Consortium via the PRIDE partner repository with the data set identifier PXD047320.

Author contribution

RB and AF designed the experiments. RB, NG and AS performed experiments and analysed the results (NG and AS equally contributed to both experiments and analyses). FT, CA, EM, CC performed specific experiments. GT and MB analysed specific results. SV and CT performed statistical analyses. RB and AF wrote the manuscript with helpful revision by AR, GT, AL and EM. All the authors have read and approved the manuscript.

Acknowledgements

We thank Dr. Patrizia Vaghi and Dr. Amanda Oldani, Centro Grandi Strumenti, University of Pavia, Italy, for the confocal analysis support; Dr. Samantha Solito and Dr. Alberto Azzalin, Centro Grandi Strumenti, University of Pavia, Italy, for the FACS technical support; the animal facility "Centro di servizio per la gestione unificata delle attività di stabulazione e di radiobiologia" of the University of Pavia, Pavia, Italy to host the animals; the OPBA of the University of Pavia for support with animal protocol. The SP1.D8 monoclonal antibody was obtained from the Developmental Studies Hybridoma Bank, created by the NICHD of the NIH and maintained at The University of Iowa, Department of Biology, Iowa City, IA 52242.

Conflict of interest

The authors have declared that no conflict of interest exists.

Funding

This work was supported by Italian Ministry of Education, University and Research (MIUR) [Dipartimenti di Eccellenza (2023-2027)] to AF; Fondazione Telethon grant no. GMR22T1024 to RB; MIUR PRIN2022 ERWJKZ to RB; MIUR PRIN2022 3C8C5B to AF.

References

1. Kadler KE, Baldock C, Bella J, et al. Collagens at a glance. *J Cell Sci.* 2007;120(Pt 12):1955-8.
2. Ishikawa Y, and Bächinger HP. A molecular ensemble in the rER for procollagen maturation. *Biochim Biophys Acta.* 2013;1833(11):2479-91.
3. Schwarze U, Cundy T, Pyott SM, et al. Mutations in FKBP10, which result in Bruck syndrome and recessive forms of osteogenesis imperfecta, inhibit the hydroxylation of telopeptide lysines in bone collagen. *Hum Mol Genet.* 2013;22(1):1-17.
4. Hennet T. Collagen glycosylation. *Curr Opin Struct Biol.* 2019;56:131-8.
5. Bunel L, Pincet L, Malhotra V, et al. A model for collagen secretion by intercompartmental continuities. *Proc Natl Acad Sci U S A.* 2024;121(1):e2310404120.
6. Jin L, Pahuja KB, Wickliffe KE, et al. Ubiquitin-dependent regulation of COPII coat size and function. *Nature.* 2012;482(7386):495-500.
7. Keller P, and Simons K. Post-Golgi biosynthetic trafficking. *J Cell Sci.* 1997;110 (Pt 24):3001-9.
8. Polishchuk RS, Polishchuk EV, Marra P, et al. Correlative light-electron microscopy reveals the tubular-saccular ultrastructure of carriers operating between Golgi apparatus and plasma membrane. *J Cell Biol.* 2000;148(1):45-58.
9. Polishchuk EV, Di Pentima A, Luini A, et al. Mechanism of constitutive export from the golgi: bulk flow via the formation, protrusion, and en bloc cleavage of large trans-golgi network tubular domains. *Mol Biol Cell.* 2003;14(11):4470-85.
10. Malhotra V, and Erlmann P. The pathway of collagen secretion. *Annu Rev Cell Dev Biol.* 2015;31:109-24.

718 11. Ishikawa Y, Ito S, Nagata K, et al. Intracellular mechanisms of molecular recognition
719 and sorting for transport of large extracellular matrix molecules. *Proc Natl Acad Sci U*
720 *S A.* 2016;113(41):E6036-E44.
721 12. Ishida Y, and Nagata K. Hsp47 as a collagen-specific molecular chaperone. *Methods*
722 *Enzymol.* 2011;499:167-82.
723 13. Shuster S. Osteoporosis, a unitary hypothesis of collagen loss in skin and bone. *Med*
724 *Hypotheses.* 2005;65(3):426-32.
725 14. Forlino A, and Marini JC. Osteogenesis imperfecta. *Lancet.* 2016;387(10028):1657-71.
726 15. Mao JR, and Bristow J. The Ehlers-Danlos syndrome: on beyond collagens. *J Clin*
727 *Invest.* 2001;107(9):1063-9.
728 16. Kang AH, and Trelstad RL. A collagen defect in homocystinuria. *J Clin Invest.*
729 1973;52(10):2571-8.
730 17. Marini JC, Forlino A, Bächinger HP, et al. Osteogenesis imperfecta. *Nat Rev Dis*
731 *Primers.* 2017;3:17052.
732 18. Palomo T, Fassier F, Ouellet J, et al. Intravenous Bisphosphonate Therapy of Young
733 Children With Osteogenesis Imperfecta: Skeletal Findings During Follow Up
734 Throughout the Growing Years. *J Bone Miner Res.* 2015;30(12):2150-7.
735 19. Etich J, Leßmeier L, Rehberg M, et al. Osteogenesis imperfecta-pathophysiology and
736 therapeutic options. *Mol Cell Pediatr.* 2020;7(1):9.
737 20. Papapoulos SE, and Cremers SC. Prolonged bisphosphonate release after treatment in
738 children. *N Engl J Med.* 2007;356(10):1075-6.
739 21. Alharbi M, Pinto G, Finidori G, et al. Pamidronate treatment of children with moderate-
740 to-severe osteogenesis imperfecta: a note of caution. *Horm Res.* 2009;71(1):38-44.

741 22. Nicolaou N, Agrawal Y, Padman M, et al. Changing pattern of femoral fractures in
742 osteogenesis imperfecta with prolonged use of bisphosphonates. *J Child Orthop.*
743 2012;6(1):21-7.
744 23. Sinder BP, White LE, Salemi JD, et al. Adult Brtl/+ mouse model of osteogenesis
745 imperfecta demonstrates anabolic response to sclerostin antibody treatment with
746 increased bone mass and strength. *Osteoporos Int.* 2014;25(8):2097-107.
747 24. Sinder BP, Salemi JD, Ominsky MS, et al. Rapidly growing Brtl/+ mouse model of
748 osteogenesis imperfecta improves bone mass and strength with sclerostin antibody
749 treatment. *Bone.* 2015;71:115-23.
750 25. Grafe I, Alexander S, Yang T, et al. Sclerostin Antibody Treatment Improves the Bone
751 Phenotype of Crtap(-/-) Mice, a Model of Recessive Osteogenesis Imperfecta. *J Bone*
752 *Miner Res.* 2016;31(5):1030-40.
753 26. Vestergaard Kvist A, Faruque J, Vallejo-Yagüe E, et al. Cardiovascular Safety Profile
754 of Romosozumab: A Pharmacovigilance Analysis of the US Food and Drug
755 Administration Adverse Event Reporting System (FAERS). *J Clin Med.* 2021;10(8).
756 27. Widmer C, Gebauer JM, Brunstein E, et al. Molecular basis for the action of the
757 collagen-specific chaperone Hsp47/SERPINH1 and its structure-specific client
758 recognition. *Proc Natl Acad Sci U S A.* 2012;109(33):13243-7.
759 28. Ito S, and Nagata K. Roles of the endoplasmic reticulum-resident, collagen-specific
760 molecular chaperone Hsp47 in vertebrate cells and human disease. *J Biol Chem.*
761 2019;294(6):2133-41.
762 29. Satoh M, Hirayoshi K, Yokota S, Hosokawa N, and Nagata K. Intracellular interaction
763 of collagen-specific stress protein HSP47 with newly synthesized procollagen. *J Cell*
764 *Biol.* 1996;133(2):469-83.

765 30. Besio R, Chow CW, Tonelli F, et al. Bone biology: insights from osteogenesis
766 imperfecta and related rare fragility syndromes. *FEBS J.* 2019;286(15):3033-56.
767 31. Besio R, Garibaldi N, Leoni L, et al. Cellular stress due to impairment of collagen prolyl
768 hydroxylation complex is rescued by the chaperone 4-phenylbutyrate. *Dis Model Mech.*
769 2019;12(6).
770 32. Takagi M, Ishii T, Barnes AM, et al. A novel mutation in LEPRE1 that eliminates only
771 the KDEL ER- retrieval sequence causes non-lethal osteogenesis imperfecta. *PLoS*
772 *One.* 2012;7(5):e36809.
773 33. Amor IM, Rauch F, Gruenwald K, et al. Severe osteogenesis imperfecta caused by a
774 small in-frame deletion in CRTAP. *Am J Med Genet A.* 2011;155A(11):2865-70.
775 34. Beriault DR, and Werstuck GH. Detection and quantification of endoplasmic reticulum
776 stress in living cells using the fluorescent compound, Thioflavin T. *Biochim Biophys*
777 *Acta.* 2013;1833(10):2293-301.
778 35. Arad E, Green H, Jelinek R, et al. Revisiting thioflavin T (ThT) fluorescence as a
779 marker of protein fibrillation - The prominent role of electrostatic interactions. *J Colloid*
780 *Interface Sci.* 2020;573:87-95.
781 36. Besio R, Iula G, Garibaldi N, et al. 4-PBA ameliorates cellular homeostasis in
782 fibroblasts from osteogenesis imperfecta patients by enhancing autophagy and
783 stimulating protein secretion. *Biochim Biophys Acta Mol Basis Dis.* 2018;1864(5 Pt
784 A):1642-52.
785 37. Garibaldi N, Contento BM, Babini G, et al. Targeting cellular stress in vitro improves
786 osteoblast homeostasis, matrix collagen content and mineralization in two murine
787 models of osteogenesis imperfecta. *Matrix Biol.* 2021;98:1-20.

38. Mirigian LS, Makareeva E, Mertz EL, et al. Osteoblast Malfunction Caused by Cell Stress Response to Procollagen Misfolding in α2(I)-G610C Mouse Model of Osteogenesis Imperfecta. *J Bone Miner Res.* 2016;31(8):1608-16.

39. Galluzzi L, Bravo-San Pedro JM, Levine B, et al. Pharmacological modulation of autophagy: therapeutic potential and persisting obstacles. *Nat Rev Drug Discov.* 2017;16(7):487-511.

40. Drzewiecki KE, Grisham DR, Parmar AS, et al. Circular Dichroism Spectroscopy of Collagen Fibrillogenesis: A New Use for an Old Technique. *Biophys J.* 2016;111(11):2377-86.

41. Tonelli F, Cotti S, Leoni L, et al. Crtap and p3h1 knock out zebrafish support defective collagen chaperoning as the cause of their osteogenesis imperfecta phenotype. *Matrix Biol.* 2020;90:40-60.

42. Valli M, Barnes AM, Gallanti A, et al. Deficiency of CRTAP in non-lethal recessive osteogenesis imperfecta reduces collagen deposition into matrix. *Clin Genet.* 2012;82(5):453-9.

43. Caparrós-Martin JA, Valencia M, Pulido V, et al. Clinical and molecular analysis in families with autosomal recessive osteogenesis imperfecta identifies mutations in five genes and suggests genotype-phenotype correlations. *Am J Med Genet A.* 2013;161A(6):1354-69.

44. Lisse TS, Thiele F, Fuchs H, et al. ER stress-mediated apoptosis in a new mouse model of osteogenesis imperfecta. *PLoS Genet.* 2008;4(2):e7.

45. Gioia R, Panaroni C, Besio R, et al. Impaired osteoblastogenesis in a murine model of dominant osteogenesis imperfecta: a new target for osteogenesis imperfecta pharmacological therapy. *Stem Cells.* 2012;30(7):1465-76.

46. Bini L, Schvartz D, Carnemolla C, et al. Intracellular and Extracellular Markers of Lethality in Osteogenesis Imperfecta: A Quantitative Proteomic Approach. *Int J Mol Sci.* 2021;22(1).

47. Fabre S, Funck-Brentano T, and Cohen-Solal M. Anti-Sclerostin Antibodies in Osteoporosis and Other Bone Diseases. *J Clin Med.* 2020;9(11).

48. Aditya S, and Rattan A. Sclerostin Inhibition: A Novel Target for the Treatment of Postmenopausal Osteoporosis. *J Midlife Health.* 2021;12(4):267-75.

49. Tie Y, Tang F, Peng D, et al. TGF-beta signal transduction: biology, function and therapy for diseases. *Mol Biomed.* 2022;3(1):45.

50. Scheiber AL, Wilkinson KJ, Suzuki A, et al. 4PBA reduces growth deficiency in osteogenesis imperfecta by enhancing transition of hypertrophic chondrocytes to osteoblasts. *JCI Insight.* 2022;7(3).

51. Duran I, Zieba J, Csukasi F, et al. 4-PBA Treatment Improves Bone Phenotypes in the Aga2 Mouse Model of Osteogenesis Imperfecta. *J Bone Miner Res.* 2022;37(4):675-86.

52. Gioia R, Tonelli F, Ceppi I, et al. The chaperone activity of 4PBA ameliorates the skeletal phenotype of Chihuahua, a zebrafish model for dominant osteogenesis imperfecta. *Hum Mol Genet.* 2017;26(15):2897-911.

53. Raote I, Saxena S, and Malhotra V. Sorting and Export of Proteins at the Endoplasmic Reticulum. *Cold Spring Harb Perspect Biol.* 2023;15(5).

54. Koide T, Asada S, Takahara Y, et al. Specific recognition of the collagen triple helix by chaperone HSP47: minimal structural requirement and spatial molecular orientation. *J Biol Chem.* 2006;281(6):3432-8.

835 55. Nagai N, Hosokawa M, Itohara S, et al. Embryonic lethality of molecular chaperone
836 hsp47 knockout mice is associated with defects in collagen biosynthesis. *J Cell Biol.*
837 2000;150(6):1499-506.
838 56. Christiansen HE, Schwarze U, Pyott SM, et al. Homozygosity for a missense mutation
839 in SERPINH1, which encodes the collagen chaperone protein HSP47, results in severe
840 recessive osteogenesis imperfecta. *Am J Hum Genet.* 2010;86(3):389-98.
841 57. Taguchi T, and Razzaque MS. The collagen-specific molecular chaperone HSP47: is
842 there a role in fibrosis? *Trends Mol Med.* 2007;13(2):45-53.
843 58. Xiong G, Chen J, Zhang G, et al. Hsp47 promotes cancer metastasis by enhancing
844 collagen-dependent cancer cell-platelet interaction. *Proc Natl Acad Sci U S A.*
845 2020;117(7):3748-58.
846 59. Jia J, Yue X, Zhu L, et al. KDEL receptor is a cell surface receptor that cycles between
847 the plasma membrane and the Golgi via clathrin-mediated transport carriers. *Cell Mol*
848 *Life Sci.* 2021;78(3):1085-100.
849 60. Shomron O, Nevo-Yassaf I, Aviad T, et al. COPII collar defines the boundary between
850 ER and ER exit site and does not coat cargo containers. *J Cell Biol.* 2021;220(6).
851 61. Aridor M. A tango for coats and membranes: New insights into ER-to-Golgi traffic.
852 *Cell Rep.* 2022;38(3):110258.
853 62. Tasab M, Batten MR, and Bulleid NJ. Hsp47: a molecular chaperone that interacts with
854 and stabilizes correctly-folded procollagen. *EMBO J.* 2000;19(10):2204-11.
855 63. Syx D, Ishikawa Y, Gebauer J, et al. Aberrant binding of mutant HSP47 affects
856 posttranslational modification of type I collagen and leads to osteogenesis imperfecta.
857 *PLoS Genet.* 2021;17(2):e1009339.
858 64. Banushi B, Forneris F, Straatman-Iwanowska A, et al. Regulation of post-Golgi LH3
859 trafficking is essential for collagen homeostasis. *Nat Commun.* 2016;7:12111.

65. Fokkema IF, Taschner PE, Schaafsma GC, et al. LOVD v.2.0: the next generation in gene variant databases. *Hum Mutat.* 2011;32(5):557-63.

66. de Vlaming A, Sauls K, Hajdu Z, et al. Atrioventricular valve development: new perspectives on an old theme. *Differentiation.* 2012;84(1):103-16.

67. McNeeley MF, Dontchos BN, Laflamme MA, et al. Aortic dissection in osteogenesis imperfecta: case report and review of the literature. *Emerg Radiol.* 2012;19(6):553-6.

68. Rauch F, and Morin SN. Transition from Pediatric to Adult Health Care in Osteogenesis Imperfecta. *Curr Osteoporos Rep.* 2023;21(4):426-32.

69. Nyström A, Bruckner-Tuderman L, and Kiritsi D. Dystrophic Epidermolysis Bullosa: Secondary Disease Mechanisms and Disease Modifiers. *Front Genet.* 2021;12:737272.

70. Spranger J, Winterpacht A, and Zabel B. The type II collagenopathies: a spectrum of chondrodysplasias. *Eur J Pediatr.* 1994;153(2):56-65.

71. Paganini C, Gramegna Tota C, Monti L, et al. Improvement of the skeletal phenotype in a mouse model of diastrophic dysplasia after postnatal treatment with N-acetylcysteine. *Biochem Pharmacol.* 2021;185:114452.

72. Jariashvili K, Madhan B, Brodsky B, et al. UV damage of collagen: insights from model collagen peptides. *Biopolymers.* 2012;97(3):189-98.

73. Knuutinen A, Kokkonen N, Risteli J, et al. Smoking affects collagen synthesis and extracellular matrix turnover in human skin. *Br J Dermatol.* 2002;146(4):588-94.

74. Jorgensen LN, Kallehave F, Christensen E, et al. Less collagen production in smokers. *Surgery.* 1998;123(4):450-5.

75. Gullahorn L, Lippiello L, and Karpman R. Smoking and osteoarthritis: differential effect of nicotine on human chondrocyte glycosaminoglycan and collagen synthesis. *Osteoarthritis Cartilage.* 2005;13(10):942-3.

76. Mottes M, Gomez Lira M, Zolezzi F, et al. Four new cases of lethal osteogenesis imperfecta due to glycine substitutions in COL1A1 and genes. Mutations in brief no. 152. Online. *Hum Mutat.* 1998;12(1):71-2.

77. Forlino A, Tonelli F, and Besio R. Steady-State and Pulse-Chase Analyses of Fibrillar Collagen. *Methods Mol Biol.* 2019;1952:45-53.

78. Mortarino M, Tedeschi G, Negri A, et al. Two-dimensional polyacrylamide gel electrophoresis map of bull seminal plasma proteins. *Electrophoresis.* 1998;19(5):797-801.

79. Eberini I, Calabresi L, Wait R, et al. Macrophage metalloproteinases degrade high-density-lipoprotein-associated apolipoprotein A-I at both the N- and C-termini. *Biochem J.* 2002;362(Pt 3):627-34.

80. Toni M, Angiulli E, Miccoli G, et al. Environmental temperature variation affects brain protein expression and cognitive abilities in adult zebrafish (Danio rerio): A proteomic and behavioural study. *J Proteomics.* 2019;204:103396.

Legends

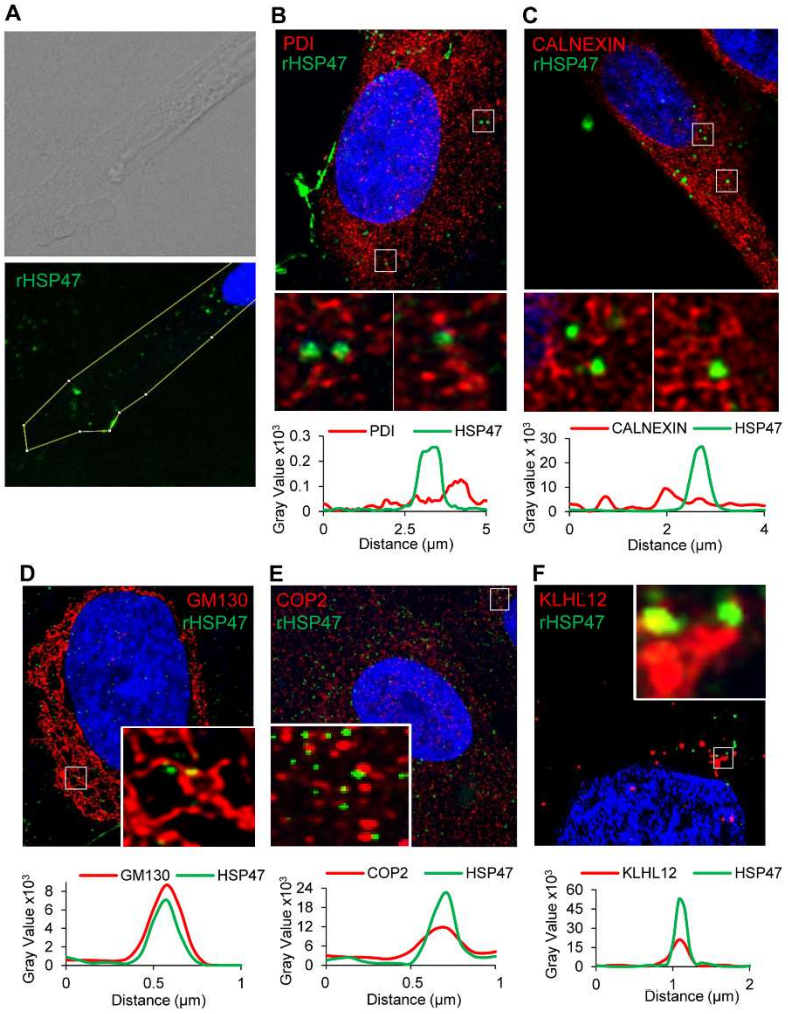

Figure 1. Recombinant heat shock protein 47 (rHSP47) is up taken by human fibroblasts. (**A**) The intracellular uptake and presence of rHSP47-GFP^{+} is shown by bright field and immunofluorescence (n=3, representative image is shown). (**B-C**) Immunofluorescence representative images of primary wild type fibroblasts incubated with rHSP47-GFP^{+} and stained with the ER markers protein disulfide isomerase (PDI) and calnexin (n=3), (**D**) with the *cis*-Golgi marker Golgi matrix protein 130 (GM130) and with markers of the secretory vesicles (n=3) (**E**) coat protein complex 2 (COP2) (n=3) and (**F**) kelch like family member 12 (KLHL12) (n=3). Colocalization of rHSP47-GFP^{+} with *cis*-Golgi and secretory vesicles, but

not with ER, is indicated by the overlapping peaks in the graphs. Nuclei were counterstained with DAPI.

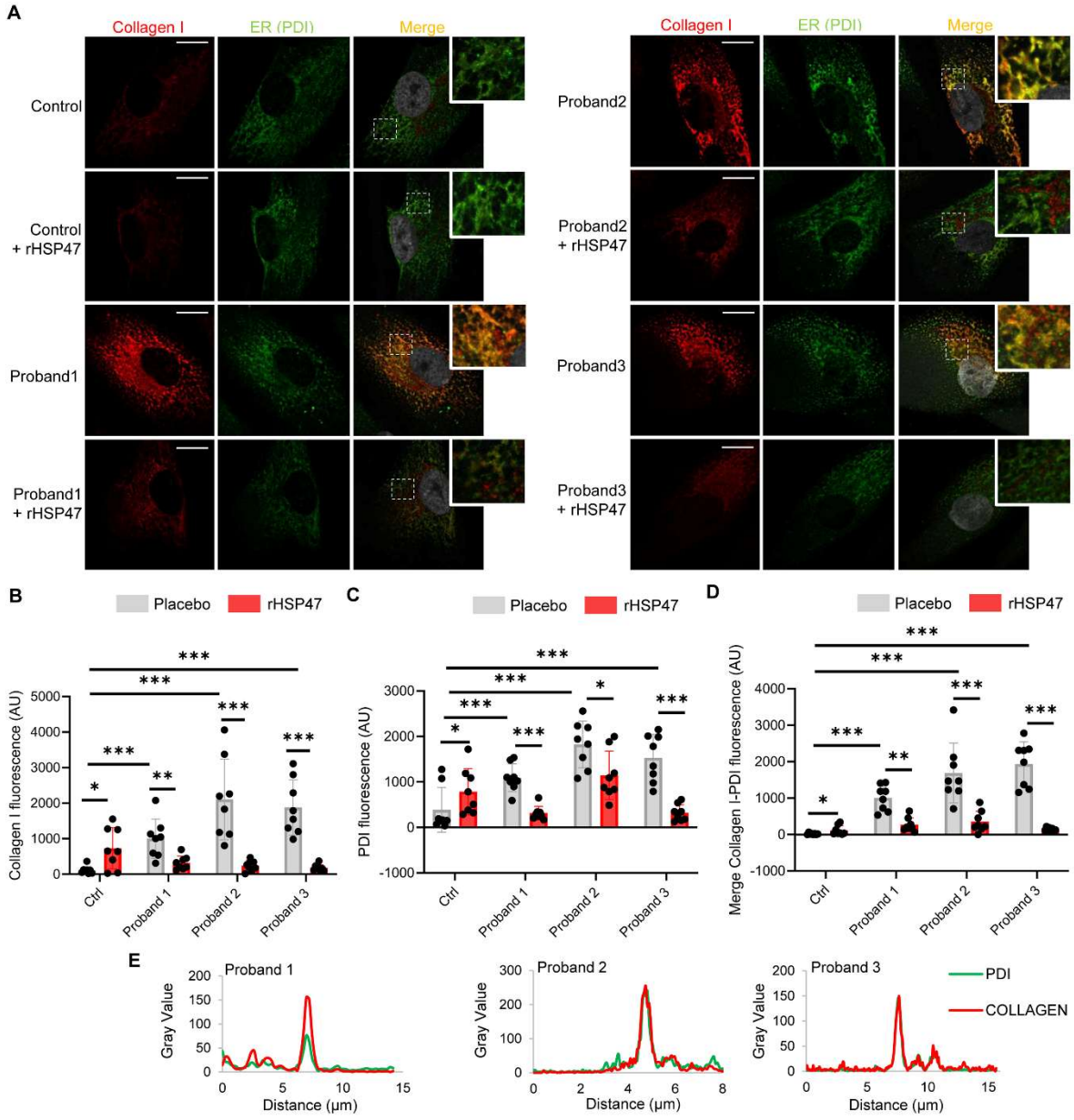

921

922 **Figure 2. Treatment with recombinant heat shock protein 47 (rHSP47) reduces**

923 **intracellular procollagen retention.**

924 (**A**) Representative images and quantification of immunofluorescence of (**B**) collagen I

925 (Aligned rank ANOVA test, F_{ARA}=18.06, p<0.001), (**C**) ER marker protein disulfide isomerase

926 (PDI) (ARA test, F_{ARA}=15.12, p<0.001), and of (**D**) collagen I-PDI signal (ARA test,

927 F_{ARA}=40.35, p<0.001) of osteogenesis imperfecta (OI) proband and control fibroblasts treated

928 for 16 h with 0.5 µM rHSP47 or with placebo. Biological replicates (n=3) were performed. For

929 each biological replicate, the signal was quantified on 8 images (40x) for each

930 genotype/condition (number of cells> 90). Error bars indicate SD. (**E**) The colocalization of
931 collagen I-PDI signal in proband 1, 2 and 3 cells is evident by the two overlapping peaks in the
932 graph (n=3). Nuclei were counterstained with DAPI. Scale bar: 15 μm. Insets showcase
933 enlarged areas. Statistical analyses details are reported in Supplementary Table S2. *$p<0.05$,
934 ** $p\leq0.01$,*** $p\leq0.001$.
935

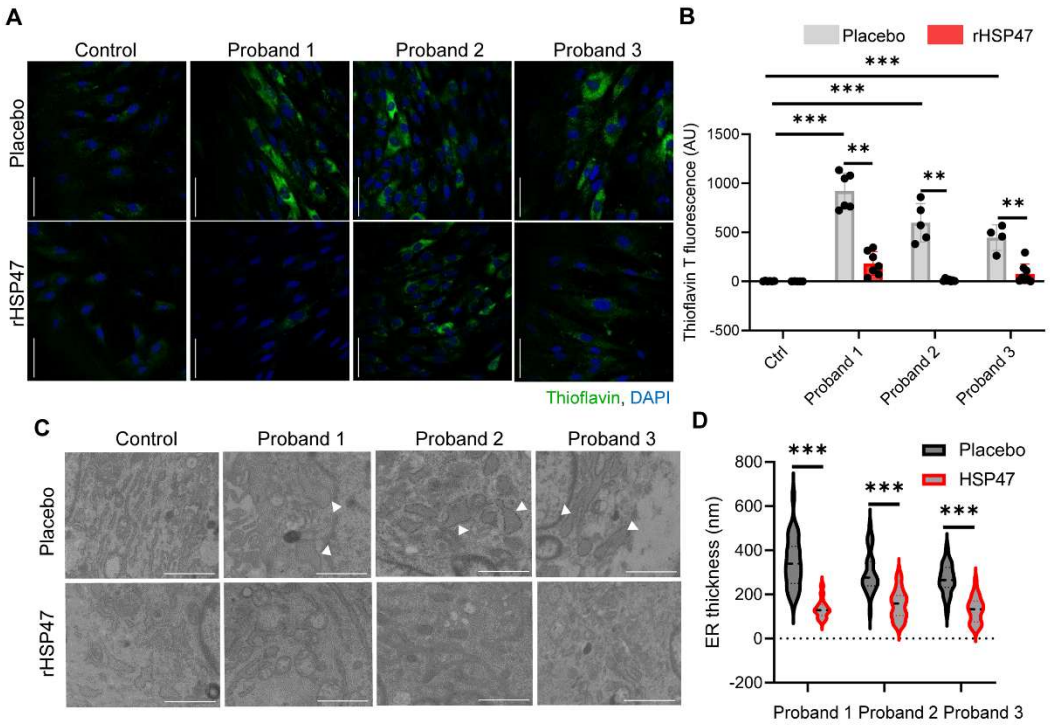

936

937 **Figure 3. Recombinant heat shock protein 47 (rHSP47) ameliorates cellular homeostasis.**
938 ER proteostasis was evaluated by thioflavin T (ThT) labelling of protein aggregates in
939 osteogenesis imperfecta (OI) proband and control fibroblasts treated for 16 h with 0.5 µM
940 rHSP47 or with placebo. (**A**) Representative immunofluorescence images and (**B**) ThT
941 quantification (Aligned rank ANOVA test, F_{ARA}=86.82, p<0.001) are shown. Biological
942 replicates (n =3) were performed. For each biological replicate, the signal was quantified on 7
943 images (40x) for each genotype/condition (number of cells> 70). Error bars indicate SD. Scale
944 bar: 20 µm. (**C**) Transmission electron microscopy representative images of OI probands and
945 control fibroblasts treated for 16 h with 0.5 µM rHSP47 or with placebo (n=3). Arrowheads
946 show ER enlargement. Scale bar: 2 µm. (**D**) ER enlargement thickness was quantified on 30
947 proband cells treated with rHSP47 or with placebo (Mann Whitney Wilcoxon test, MW=6.35,
948 p<0.001). Statistical analyses details are reported in Supplementary Table S2. ** p≤0.01, ***
949 p≤0.001.

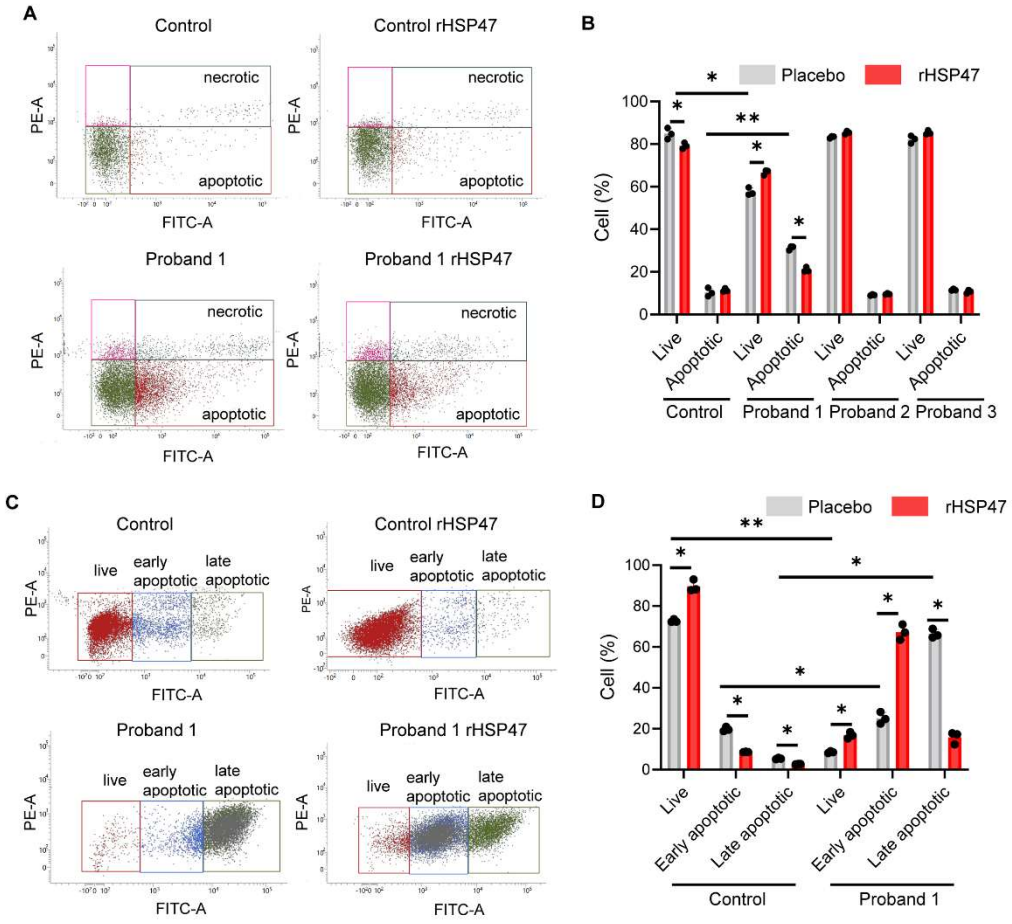

950

951 **Figure 4. Recombinant heat shock protein 47 (rHSP47) modulates cell apoptosis.**

952 (**A**) FACS analysis detection of apoptotic cells in OI probands and control fibroblasts treated
953 with rHSP47 or with placebo following annexin V (FITC) and propidium iodide (PI) staining.
954 The fraction of apoptotic events in the cells is shown in representative plots and (**B**) quantified
955 in the histogram. Biological replicates (n=3) were performed. Error bars indicate SD. (**C**)
956 FACS analysis detection of apoptotic cells in OI proband 1 and control fibroblasts treated with
957 rHSP47 or with placebo following a high stress condition induced by culturing the cells for 7
958 days without media change. The fraction of apoptotic events in the cells is shown in
959 representative plots and (**D**) quantified in the histogram. Both early and late apoptotic cells
960 were quantified. Biological replicates (n =3) were performed. Error bars indicate SD. Mann
961 Whitney Wilcoxon test was performed. Statistical analyses details are reported in
962 Supplementary Table S2. *$p<0.05$, **$p\leq0.01$.

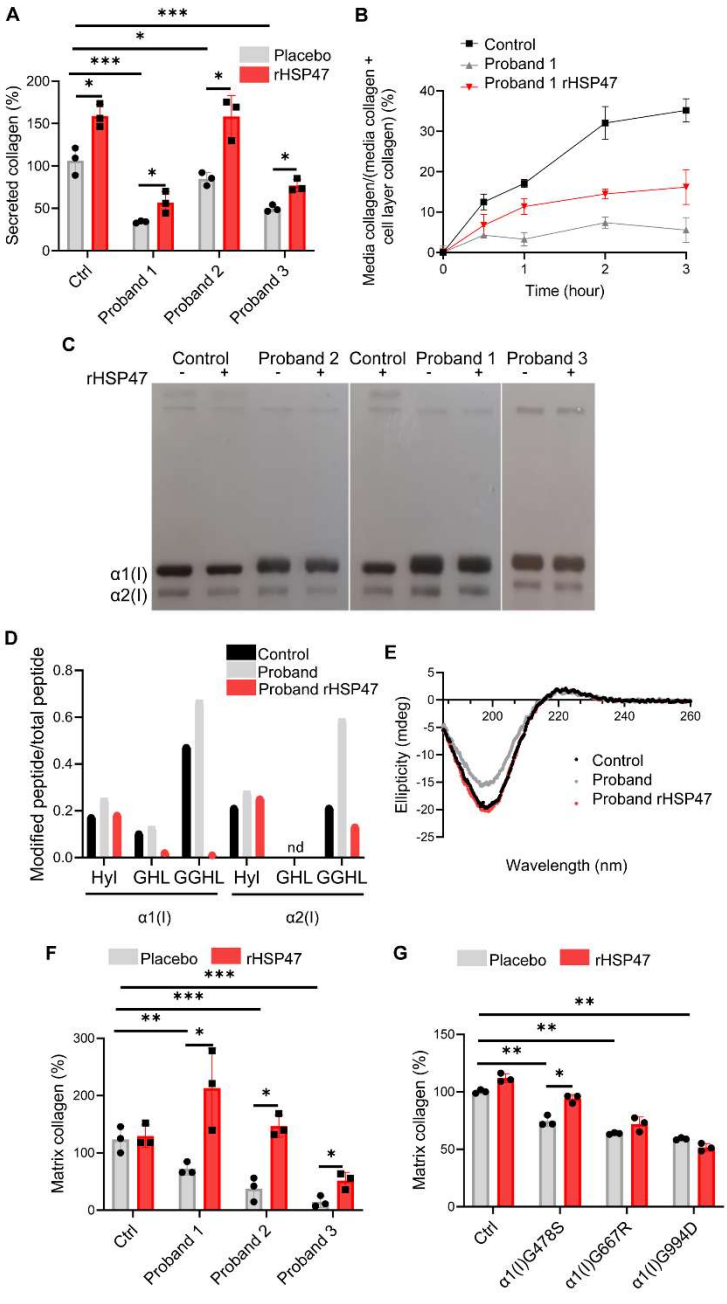

963

964 **Figure 5. Recombinant heat shock protein 47 (rHSP47) increases collagen secretion,**
965 **reduces collagen overmodifications and enhances collagen I deposition in the**
966 **extracellular matrix.**

967 (**A**) rHSP47 effect on collagen secretion was evaluated in osteogenesis imperfecta (OI)
968 probands and control fibroblasts. Secreted collagen was quantified in the last 24 h culture media
969 of fibroblasts after 7 days of culture with or without 4 h rHSP47 pulse (0.5 µM) every other
970 day. Biological replicates (n=3) were performed. For each biological replicate, collagen was

quantified in 3 different wells for each condition. Kruskal-Wallis (KW) test, KW=17.93, P=0.0005. (**B**) Collagen secretion kinetics was evaluated in proband 1 by incubating the cells for 4 h with ^{3}H-proline. Technical replicates (n=3) were performed. (**C**) Representative SDS-urea-PAGE of ^{3}H-labeled collagen extracted from the medium of control and OI probands' fibroblasts treated for 16 h with 0.5 μM rHSP47 or with placebo. Biological replicates (n=3) were performed. (**D**) Tandem mass spectrometry data of collagen I extracted from culture media of control and proband fibroblasts to evaluate lysyl hydroxylation and lysine O-glycosylation along the collagen helix (n=3, pooled). Hydroxylysine (Hyl), galactosyl-hydroxylysine (GHL) and glucosylgalactosyl-hydroxylysine (GGHL) sites were identified by the analysis. The ratio between the post translational modified peptides and the total peptides is reported. (**E**) Circular dichroism spectra reveal the collagen triple helix signal as a positive peak at 222 nm and negative peak below 200 nm in all samples (n=3). (**F**) The amount of collagen incorporated into the extracellular matrix (ECM) was evaluated by picro sirius red staining in cells grown for 7 days in absence or presence of 0.5 μM rHSP47 4 h pulse performed every other day. Biological replicates (n=3) were performed. For each biological replicate, collagen was quantified in 3 different wells for each condition. (**G**) The amount of collagen incorporated into the ECM was evaluated in fibroblasts from probands with collagen I mutations as reported in F (n=3). Error bars indicate SD. Mann Whitney Wilcoxon test was applied. Kruskal-Wallis (KW) test was also applied to describe the secreted collagen by genotype. Statistical analyses in Supplementary Table S2. *$p<0.05$, **$p\leq0.01$, **$p\leq0.01$.

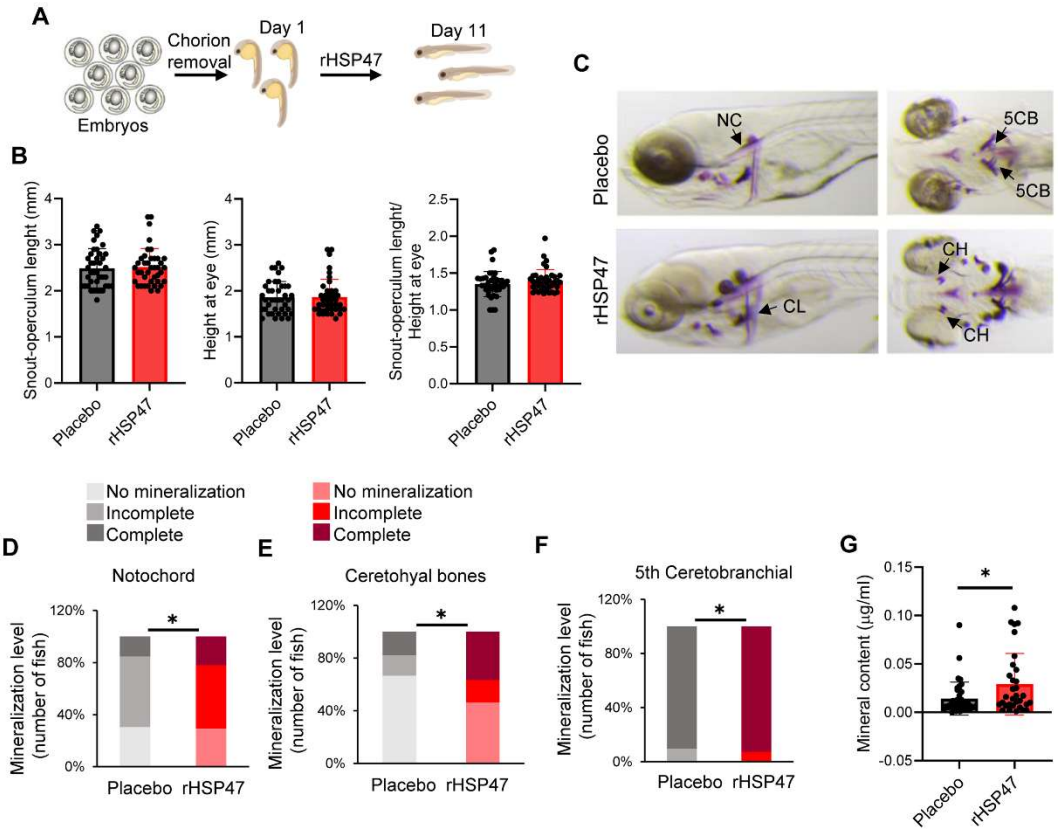

Figure 6. Treatment with recombinant heat shock protein 47 (rHSP47) ameliorates zebrafish *p3h1*$^{-/-}$ larvae bone mineralization.

(**A**) Upon mechanical chorion removal, embryos from prolyl-3-hydroxylase 1 knock out zebrafish (*p3h1*$^{-/-}$) were treated every other day with a 4 h pulse of 0.5 µM rHSP47 or with placebo. At 11 dpf the skeleton of larvae was stained with alizarin red in order to assess the rHSP47 effect on mineralization. (**B**) Analysis of the fish morphology was carried out measuring the snout-operculum length, the height at eye and the ratio snout-operculum length/ height at eye (n=40). (**C**) Lateral and ventral images of *p3h1*$^{-/-}$ larvae, treated with rHSP47 or placebo, upon mineral staining by alizarin red. (**D-E-F**) Bone mineralization level analysed in rHSP47 treated and untreated fish. Three classes of mineralization were defined, namely no mineralization, incomplete and complete, based on the level of alizarin red staining. Biological replicates (n=41) were performed. (**G**) Total larvae mineral content was extracted and quantified by spectrophotometric analyses. Biological replicates (n=32) were performed. Error

1005 bars indicate SD. Mann Whitney Wilcoxon test was applied. Statistical analyses details are
1006 reported in Supplementary Table S2. **$p \leq 0.01$.
1007
1008

Table1: List of the probands primary fibroblasts used in the study.

Proband	Gene	Protein	Gene mutation	Protein mutation	OI type	Clinical phenotype
Proband 1	*P3H1*	P3H1	c.765C>A/ c.2055+18G>A	Tyr255Ter Not reported	VIII	Severe skeletal dysplasia characterized by short, bowed and deformed long bones
Proband 2	*P3H1*	P3H1	c.2148delC/c.2148delC	Glu719Asnfs*747	VIII	Short stature, long bone fractures and deformities, vertebral deformities, osteopenia
Proband 3	*CRTAP*	CRTAP	c.804_809delAGAAGT/ c.804_809delAGAAGT	Glu269_Val270del	VII	Short stature, long bone fractures and deformities, rib fractures, vertebral deformities, compression and fractures, scoliosis, osteopenia, no rizhomelia, grayish sclerae

Table 2. MS/MS analysis of Hyl, GHL and GGHL of α1(I) and α2(I) extracted from control fibroblasts, OI fibroblasts and OI fibroblasts treated with rHSP47.

For each lysine site identified, the table reports the peak intensity of the hydroxylated (Hyl), mono-*O*-glycosylated (GHL) and di-*O*-glycosylated (GGHL) peptides and of the corresponding unmodified peptides. The ratio between the intensity of the modified peptides and the total intensity of all peptide's forms (unmodified + hydroxylated + mono-*O*-glycosylated + di-*O*-glycosylated) is indicated. In grey the sum of the peak intensity of the modified and unmodified peptides, and the ratio of the modified/total is highlighted.

Nd, not detected; Hyl, hydroxylysine; GHL, galactosylhydroxy-lysine; GGHL, glucosylgalactosylhydroxylysine.

		Modified peptides			**Unmodified peptides**			**Ratio modified/total**		
Modification Lysine site*	**α1(I)**	**Control**	**OI**	**HSP47**	**Control**	**OI**	**HSP47**	**Control**	**OI**	**HSP47**
Hyl	K^{252}	9.58E+09	1.40E+10	3.47E+07	3.22E+09	1.13E+09	7.91E+04	0.75	0.93	1.00
	K^{270}	6.27E+08	9.19E+08	7.12E+06	Nd	Nd	Nd	Nd	Nd	Nd
	K^{327}	6.29E+09	6.66E+09	1.84E+07	8.75E+10	7.21E+10	5.35E+07	0.07	0.08	0.26
	K^{603}	2.02E+09	3.03E+09	3.89E+08	1.61E+09	4.26E+09	2.05E+09	0.56	0.42	0.16
	Total	1.85E+10	2.46E+10	4.49E+08	9.24E+10	7.75E+10	2.10E+09	0.17	0.24	0.18
	Total (%)							100%	141%	105%
GHL	K^{99}	3.90E+09	3.48E+09	1.06E+07	3.71E+10	2.54E+10	6.80E+08	0.10	0.12	0.02
	Total	3.90E+09	3.48E+09	1.05E+07	3.71E+10	2.54E+10	6.80E+08	0.10	0.12	0.02
	Total (%)							100%	120%	20%
GGHL	K^{87}	6.64E+10	8.11E+10	1.60E+07	1.54E+06	1.08E+08	2.33E+04	1.00	1.00	1.00
	K^{99}	1.21E+09	2.66E+09	1.93E+08	3.71E+10	2.54E+10	6.80E+08	0.03	0.09	0.22
	K^{408}	3.94E+09	9.62E+09	2.42E+07	4.58E+10	2.25E+10	2.83E+10	0.079	0.299	0.001
	K^{855}	1.21E+09	7.45E+08	1.52E+07	1.13E+07	6.14E+06	9.32E+05	0.99	0.99	0.94

	Total	7.28E+10	9.41E+10	2.48E+08	8.28E+10	4.81E+10	2.90E+10	0.47	0.66	0.01
	Total (%)							100%	140.4%	2.1%
	α2(I)	**Control**	**OI**	**HSP47**	**Control**	**OI**	**HSP47**	**Control**	**OI**	**HSP47**
Hyl	K^{264}	8.22E+07	1.51E+08	8.79E+04	2.15E+10	1.37E+10	1.60E+10	0.004	0.011	0.00001
	K^{270}	8.22E+07	1.51E+08	8.79E+04	4.03E+09	2.23E+09	3.31E+09	0.02	0.06	0.00003
	K^{408}	1.83E+10	1.82E+10	2.07E+10	4.23E+10	3.38E+10	4.47E+10	0.30	0.35	0.32
	K^{567}	2.28E+08	3.86E+08	5.65E+08	7.05E+08	5.50E+08	9.19E+08	0.24	0.41	0.38
	Total	1.87E+10	1.88E+10	2.13E+10	6.86E+10	5.03E+10	6.50E+10	0.21	0.27	0.25
	Total (%)							100%	128.6%	119%
GHL		Nd								
GGHL	K^{87}	8.13E+09	2.93E+10	4.04E+09	1.04E+08	7.65E+08	4.65E+08	0.99	0.97	0.90
	K^{264}	6.94E+07	1.55E+08	4.95E+06	2.37E+10	1.58E+10	1.86E+10	0.0029	0.0097	0.0003
	K^{564}	5.98E+06	4.07E+07	2.43E+07	9.40E+08	1.08E+09	2.03E+09	0.01	0.04	0.01
	K^{648}	4.15E+08	1.08E+09	3.54E+08	6.89E+09	4.86E+09	8.32E+09	0.06	0.18	0.04
	Total	8.62E+09	3.06E+10	4.43E+09	3.17E+10	2.25E+10	2.94E+10	0.21	0.58	0.13
	Total (%)							100%	276.2%	61.9%

1022

1023

Supplementary material

Table S1. **Results of LC-MS/MS analysis of hydroxylated and O-glycosylated peptides of type I collagen.** The table reports the list of hydroxylated and O-glycosylated lysine sites identified in α1(I) and α2(I) chains from control, OI and rHSP47 treated OI proband fibroblasts. Each residue is associated to the peak intensity of the peptides hydroxylated (Hyl), mono-O-glycosylated (GHL) and di-O-glycosylated (GGHL) and of the corresponding unmodified peptides. Nd, not detected; Hyl, hydroxylysine; GHL, galactosylhydroxy-lysine; GGHL, glucosylgalactosylhydroxylysine.

Table S2. **Replicates and p value analysed by aligned rank ANOVA (ARA), Mann Whitney Wilcoxon (MW), and Kruskal-Wallis (KW) test.**